CORA Cork Open Research Archive
Cartlann Taighde Oscailte Chorcaí

Title	NiO hybrid nanoarchitecture-based pseudocapacitor in organic electrolyte with high rate capability and cycle life
Author(s)	Padmanathan, Narayanasamy; Selladurai, Subramanian; Rahulan, K. Mani; O'Dwyer, Colm; Razeeb, Kafil M.
Publication date	2015-04-26
Original citation	Padmanathan, N., Selladurai, S., Rahulan, K. M., O'Dwyer, C. and Razeeb, K. M. (2015) 'NiO hybrid nanoarchitecture-based pseudocapacitor in organic electrolyte with high rate capability and cycle life', Ionics, 21(9), pp. 2623-2631. doi: 10.1007/s11581-015-1444-9
Type of publication	Article (peer-reviewed)
Link to publisher's version	http://link.springer.com/article/10.1007/s11581-015-1444-9 http://dx.doi.org/10.1007/s11581-015-1444-9 Access to the full text of the published version may require a subscription.
Rights	**© Springer-Verlag Berlin Heidelberg 2015. This is a post-peer-review, pre-copyedit version of an article published in Ionics. The final authenticated version is available online at: http://dx.doi.org/10.1007/s11581-015-1444-9**
Item downloaded from	http://hdl.handle.net/10468/6073

Downloaded on 2019-01-07T05:46:34Z

UCC

University College Cork, Ireland
Coláiste na hOllscoile Corcaigh

NiO Hybrid Nanoarchitecture based Symmetric Supercapacitor in non-aqueous electrolytes with improved rate capability and cycle life

N. Padmanathan[a,b], S. Selladurai[b], K. Mani Rahulan[c], Colm O'Dwyer[a,d] and Kafil M. Razeeb[a]∗

[a]Tyndall National Institute, University College Cork, Dyke Parade, Lee Maltings, Cork, Ireland

[b]Ionics Lab, Department of Physics, Anna University, Chennai-600 025, India

[c]Department of Physics and Nanotechnology, SRM University, Chennai-603203, India

[d]Department of Chemistry, University College Cork, Cork, Ireland

Abstract

A three dimensional hierarchical NiO nanostructures with combined microstructure of nanoflakes and nanoflowers have been fabricated on carbon fiber cloth (CFC). Unique nano-micro structural features of NiO electrode exhibit an excellent electrochemical activity as electrode material for symmetric supercapacitors in non-aqueous organic electrolyte (1 M TEABF$_4$ in propylene carbonate). The NiO/CFC electrode showed an enhanced electrochemical activity in organic electrolyte in terms of rate capability, specific energy and power performance, as well as potential limit. The symmetric supercapacitor showed a specific capacitance of 34.9 Fg^{-1} at 1 Ag^{-1} current density. It delivered a maximum specific energy density of 19.4 Whkg^{-1} at a high power density of 1000.6 Wkg^{-1} at a constant current density of 1 Ag^{-1}. The cell is also capable of long-term cycling stability with an efficiency of 58% after 25000 cycles. This superior electrochemical activity of the NiO electrode is due to their structural benefits of well-connected hybrid nano/ mesoporous structure and rapid ion intercalation within the porous electrode surface.

Keywords: Nickel oxide, nanomaterials, flexible electrode, pseudocapacitor, supercapacitor

Corresponding Author*:

Dr. Kafil M. Razeeb

Nano Interconnection Team, Tyndall National Institute, University College Cork, Dyke Parade, Lee Maltings, Cork, Ireland. Phone: +353 21 4904078, E-mail: kafil.mahmood@tyndall.ie.

Introduction

Research on electrochemical capacitors (ECs), also known as supercapacitors (SCs), has drawn tremendous attention as high performance energy storage devices. Owing to its inimitable properties like high specific capacitance, fast charge and discharge rate, good rate capability and long cycle lifetime, supercapacitors are particularly suitable for high power applications such as hybrid electric vehicles, portable electronic devices and renewable energy systems.[1-10] However, the energy densities of the state of the art supercapacitors are still lower than the conventional batteries and that limits their large scale applications. The power performance of supercapacitors with high energy density of batteries would represent a major advance in energy storage technology but this requires promising electrode materials with featured electrochemical activity (i.e., multiple oxidation states, higher and more accessible surface area, high conductivity, etc. that affect the exchange current density). Consequently, it is difficult to find an electrode that has all the required properties optimized for efficient performance in supercapacitor. For flexible SCs, a high volumetric capacitance is possible if a high packing density and large active surface areas are realized, but these materials must also exhibit good capacitive retention and mechanical flexibility over thousands of cycles.[11] Therefore different kinds of metal/ metal oxide nanostructures have been developed as the electrode for SCs applications.[12-17] In particular, non-precious metal oxides have demonstrated tunable textural and electrochemical properties in energy related devices such as supercapacitors, fuel cells, Li-ion batteries etc.[16,17] In particular, hierarchical nano-architectured active materials such as two-dimensional (2D) nanomaterials that includes families of quasi-2D graphene and transition metal dichalcogenides[18], have witnessed resurgence in application to the development of flexible supercapacitors with better electrochemical performance.

Metal oxide nanostructures directly grown on conductive substrates have been explored as the high performance supercapacitor electrodes.[19,20] These substrates are usually made of nickel foam (NF), Titanium foil, ITO, and stainless steel (SS) and used as the binder free electrode for supercapacitor.[19-25] However these, commonly known metal current collectors suffer from low structural integrity and insufficient flexibility.[26] Also considering the weight of the metal current collectors, the gravimetric capacitance with respect to the total mass of the electrode is still very low and unsatisfactory.[27] Carbon fibre cloth (CFC) is a promising substrate with good electrical

conductivity (resistivity <20 mΩcm) and excellent chemical stability in a variety of electrolytes. Furthermore it has excellent mechanical strength, flexibility and chemical compatibility.[28] Growing active materials directly onto the conducting carbon fibre cloth substrate dove-tails with technologies such as gas diffusion layers (GDLs) used in supercapacitor application. Mono and bi-metallic oxide-based homo/hetero nanostructures on CFC have been reported for supercapacitor applications.[13-15,26-29] Among them, nickel oxide is of particular interest because of its high theoretical specific capacitance (2583 Fg^{-1} within 0.5 V), high chemical/thermal stability, environmentally benign nature, low cost and easy synthesis.[14] In parallel, the creation of smart hybrid nano-architectures with a single component is complicated and requires multiple synthesis steps. Good integration of high surface area 3D hierarchical metal oxide nano-architectures on flexible substrate with enhanced capacitance and electrochemical features is difficult and only few reports are available.[10-13] More recently, Shuang Cheng et al. designed the carbon paper supported hybrid nanonet/ nanoflower NiO for high performance pseudocapacitors and observed the improved electrochemical performance in the hybrid nanostructure based on the mass (840 Fg^{-1}).[15] In advance, Qian et al. fabricated the NiO@CFC nanosheets for high performance flexible all solid state supercapacitors in polymer gel electrolyte system and obtained the areal capacitance of 842 mFcm^{-2} at 1 mAcm^{-2}.[30] However, the formation of nano/ mesoporous hybrid NiO nano-architecture on CFC or related conductive current collectors with high electrical conductivity and long cyclic stability has not yet been achieved with NiO nanostructures in particular for organic electrolyte system.

In most cases, aqueous electrolyte was used to evaluate the electrochemical capacitance of the material. An intrinsic hydrophobic nature of the CFC significantly reduces the accessibility of the electrolyte at high rates and thereby limiting the energy and power density. However, the main drawback of these aqueous solutions as electrolyte for supercapacitor applications is their narrow cell voltage and low energy density.[30, 31] Furthermore, the devices with liquid electrolytes suffer from various issues including bulky package, corrosion in electrodes and electrolyte leakage.[32] Therefore the proper choice of electrolyte is quite important to enhance the energy and power density of the supercapacitors. Organic electrolytes such as Tetraethylammonium Tetrafluorborate (TEABF$_4$), 1-Ethyl-3-methylimidazolium tetrafluoroborate (EMIMBF$_4$) and LiClO$_4$ in propylene carbonate (PC) have a higher breakdown voltage, but have also greater

resistance than those based on aqueous solution.[33] In other words, the advantage linked to an increase on the electrolyte cell voltage is, therefore, usually countered by an increase in its resistance.

Here, we report an extremely porous NiO hierarchical nanoflake/ nanoflower hybrid architecture from interconnected ultra-thin nanocrystals on highly conductive porous carbon cloth via simple hydrothermal approach without any structure directing agent. The electrochemical characteristics of the as fabricated NiO/CFC hybrid nanostructure have been examined as a high performance supercapacitor electrode in non-aqueous electrolyte. The NiO/CFC supercapacitor has delivered a maximum specific energy density 19.4 $Whkg^{-1}$ and a high power density of 1000.6 Wkg^{-1} in 1 M $TEABF_4$/PC at a current density of 1 Ag^{-1}.

Experimental Procedure

The carbon fibre cloth (CFC) was pre-treated at 1 M HCl followed by washing with ethanol, acetone and deionized (DI) water to be used as the substrate. The growth procedure are as follows:[13] 1 M of $Ni(NO_3)_2.6H_2O$ and excess amount of urea were simultaneously dissolved in equal amount of mixed DI water and ethanol (1:1) solvents under constant stirring. After 20 min, the homogenous solution was transferred to a stainless steel autoclave containing pre-treated CFC (4×4 cm^2) and kept at 180 °C for 12 h in an oven. Finally, the CFC was separated and washed with DI water followed by oxidation at 300 °C for 3 h. The content of the NiO in the substrate was measured carefully from the weight difference of the CFC before and after the growth of NiO. Typical mass of the active electrode material was ~1 mg/cm^2.

The phase, morphology and microstructure of the CFC-supported NiO electrode was characterized using X-ray diffractometer (XRD) (Bruker D2-PHASER), high resolution scanning electron microscope (FEI 200F HRSEM), and high resolution transmission electron microscope (TECNAI HRTEM-3010 at 200 kV). The mesoporosity was examined by analysis of N_2 adsorption/desorption isotherms at 77 K using a Quantachrome Quadrasorb S*I*. Electrochemical characterization was carried out at room temperature using CHI 660C electrochemical workstation. The fabricated NiO/CFC was used as the binder-free working electrode. A three
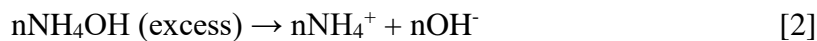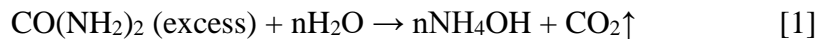
electrode cell was constructed with the NiO/CFC working electrode, Pt wire counter electrode and saturated calomel electrode (SCE) as a reference electrode. 1 M TEABF$_4$ in propylene carbonate was used as the supporting electrolyte. The sandwich type symmetric capacitors were fabricated using NiO/CFC electrodes separated by celgard separator (porosity 55%, average pore size 64 nm) and tested in the same electrolyte.

Results and Discussion

The crystalline structure of the hydrothermally grown NiO nanoflakes assembly on the CFC substrate was studied by X-ray diffraction. Figure 1a shows the XRD pattern of CFC before and after the growth of NiO. The formation of cubic NiO over the CFC surface after 300 °C calcination was confirmed. The diffraction peaks at 37.3°, 43.2° and 63° can be indexed to the (*hkl*) planes of (111), (200) and (220) of the cubic NiO crystal structure (JCPDS 47–1049).[34] The growth of NiO was further confirmed by the micro Raman spectral analysis as shown in Figure 1b. The characteristic Raman band associated with carbon (disordered carbon D-band) and graphitic carbon (G-band) as indexed in Figure 1b. The new band at ~513 cm^{-1} in the Raman spectra corresponds to Ni-O vibration consistent with the growth of NiO directly on the CFC surface.[21,35]

SEM images in Figure 2a-d show the growth of NiO nanoflakes/nanoflower hybrid microstructure on CFC substrate. Figure 2a shows the low magnification SEM image of the hybrid structure where NiO nanoflowers are grown on top of the carbon fibre and (c) shows the high magnification image of a single nanoflower. Figure 2b shows the smoother region of the fibre where NiO nanocrystals are visible and the corresponding high magnification image at (d) reveals the mesoporous structure of the carbon fibre incorporating nanocrystals and nanoflakes. It may be inferred that the ultrafine NiO nanocrystals have been assembled together and form the 3D networked hierarchical nanoflake architecture followed by the growth of typical mesoporous nanoflowers. The primary elements presented in the compound are designated by the corresponding Energy Dispersive X-ray (EDX) spectral analysis. Figure 2e clearly shows the presence of Ni, O and C elements. The inset shows the SEM micrograph of NiO

nanoflower/CFC on which EDX analysis was performed. The growth mechanism of this interesting hybrid architecture can be explained through the following chemical reactions.

$$CO(NH_2)_2 \text{ (excess)} + nH_2O \rightarrow nNH_4OH + CO_2\uparrow \qquad [1]$$

$$nNH_4OH \text{ (excess)} \rightarrow nNH_4^+ + nOH^- \qquad [2]$$

$$Ni^{2+} + 2OH^- \rightarrow Ni(OH)_2 \rightarrow NiO + H_2O \qquad [3]$$

The carbamide hydrolysis plays a crucial role in forming the networked NiO nanoflake/nanoflower microstructure. At the threshold temperature of >180 °C, urea hydrolysis followed by the extended hydrothermal treatment leads to rapid $Ni(OH)_2$ growth.[13] The excess amount of urea produces more NH_4OH that drives the solution pH above ~9. Under this basic condition, more metal hydroxide precipitate can be electrostatically attached to the CFC surface and facilitate further grow during nucleation. During nucleation, the released NH_3 is oxidized to NH_4^+ facilitating electrostatic binding to the rough, porous CFC surface that connects the nanoflakes in a disorder manner to form the 3D nanoflower architecture in addition to the nanoflakes.[36,37]

The HRTEM image of the as fabricated NiO nanostructure is shown in Figure 3a-c. Low magnification TEM images (a and b) revealed that the layered nanoflakes consist of uniformly distributed ultra-fine nanocrystals with wide range of mesopores. The porous nanoflakes connected together on the CFC substrate form the basis of the hierarchical porosity defined by the overall nanoflower growth at the top surface of the nanoflakes. Figure 3c indicates the presence of the active material delineated by the nano/ meso pores in the hybrid nanostructure. To further confirm the mesoporous structure the N_2 adsorption/desorption hysteresis was measured and discussed in next section. The selected area diffraction pattern (SAED) of lattice-resolved HRTEM data in Figure 3d confirms a lattice spacing of ~0.21 nm for (200) and ~0.47 nm for (220) planes characteristic of crystalline NiO in a polycrystalline arrangement on several length scales on the CFC surface.

As the primary contributor to pseudo and super capacitive behaviour, particularly at high current density, the mesoporous nature of the hierarchically structured self-assembled NiO nanoflakes

was examined by N_2 adsorption/desorption method as shown in Figure 4. Unique hysteresis loop of the adsorption/desorption isotherms with respect to the relative pressure confirms significant mesoporous characteristics of the NiO.[38] The estimated Brunauer−Emmett−Teller (BET) surface area is 145.75 m^2g^{-1}. The inset in Figure 4 illustrates the Barret−Joyner−Halenda (BJH) pore size distribution of the NiO nanostructure with maxima at 1.55 nm and 2.87 nm correspond to pore volumes of 0.32 and 0.52 cm^3g^{-1}, respectively. This result demonstrates that the NiO nanoflakes/nanoflower hybrid structure has a large surface area, optimized for performance at high applied current density.

High rate pseudocapacitive behaviour of the CFC supported NiO hierarchical nanoflake assembly was evaluated with cyclic voltammetry and galvanostatic charge-discharge measurements. The NiO/CFC electrode was tested with the conventional three electrode configuration in 1 M $TEABF_4$/PC, to examine the electrochemical property. The CV curves of the NiO/CFC electrode measured at scan rates from 5 to 50 mVs^{-1} are shown in Figure 5a. The electrode exhibits a pseudocapacitive behaviour with featureless current responses in their CV curves. It should be noted that the current responses of the electrode in 1 M $TEABF_4$/PC are attributed to the redox reaction over the NiO surface due to adsorption of electrolyte ions. The visible pair of redox peaks over the potential range further supports the typical pseudocapacitive nature of the NiO electrode. While adsorption of the electrolyte ion the oxidation of $Ni^{2+} \leftrightarrow Ni^{3+}$ has observed for the scan rates ranging from 5 to 20 mVs^{-1}. However, due to the larger size electrolyte ions, which do not penetrate to core active sites of the electrode, the redox peaks similar to the conventional alkaline electrolyte system is not visible. The peak current increases linearly with the square root of the scan rate in line with the Randles-Ševčík dynamics, indicating diffusion controlled faradaic reactions and confirms the high rate transportation of the electrons and ions within the electrode. When the scan rate increases to 10 times the initial rate (5 mVs^{-1}), the potential differences (ΔE_a - ΔE_c) between the redox peaks have increased significantly, which indicate a quasi-reversible redox reaction on the electrode surface with limited ionic diffusion rate. Typical charge-discharge curve over the potential range of -1 to - 1.5 V with different current density ranging from 5 to 30 Ag^{-1} for NiO electrode in organic electrolyte is shown in Figure 5b. The non-linear charging and discharging curves indicates the pseudocapacitive characteristic of the electrode. From the charge-discharge graph, the specific capacitance of the

electrode was calculated for the corresponding current rate using the relation $C = \frac{1}{mv(V_c - V_a)} \int_{V_a}^{V_c} I(V)dV \sim I\Delta t / m\Delta V$ where, I is the charge/ discharge current, t is discharge time between the potential limit (1.5-IR_{drop}) to -1, V_c - V_a is the potential difference between cathodic and anodic peaks excluding IR_{drop}, and m is the weight of the active material. The estimated C_s values range from 170 to 53 Fg^{-1} for the respective current densities of 5 and 30 Ag^{-1} (see Fig. 5). The rate capability of the electrode in non-aqueous electrolyte is limited to 30 A g^{-1} due to the increased interfacial resistance between the electrode and electrolyte, which may be arises mainly from the larger size electrolyte ion (Et$_4$N+, BF$_4$ in PC ~ 1.4 nm)[39] intercalation during redox process.[32] The electrochemical stability of the electrode material in non-aqueous electrolyte was tested by continuous charging-discharging measurement over 2500 cycles. Figure 5c shows the cyclic stability the NiO electrode in 1 M TEABF$_4$/PC and the inset represents the repeated charge/discharge profile measured at a constant current density of 20 A g^{-1}. From the graph, it can be seen that the NiO/CFC hybrid electrode exhibits an excellent cyclic stability in organic electrolyte and retain the ~ 88% of its initial capacitance at the end of 2500 cycles. In order to understand the electrode kinetics and internal resistance of the electrode, the electrochemical impedance spectral analysis was performed. A typical EIS plot for NiO/CFC electrode measured after the 1st and 2500th cycles in organic electrolyte is shown in Figure 5d. The distinct EIS spectra with high solution resistance indicate the characteristic feature of the organic electrolyte system and limited diffusion kinetics within the electrode surface. The incomplete semicircle portion infers the frequency limitation of measurement. However, the diameter of the semicircle is considerably small even after 2500 cycles, indicating the low charge transfer resistance, which demonstrates good electrical conductivity of the electrode in organic electrolyte.

To understand the capacitive characteristic of NiO/CFC electrode in non-aqueous electrolyte, a two electrode cell was constructed using NiO nanoflake/nanoflower hybrid electrodes and tested in organic (TEABF$_4$/PC) electrolyte over the wide range of potentials, both in positive and negative regions. Typical CV curves were measured at different potential limits of -2 to 0 and 0 to +2 V at a scan rate of 100 mV s^{-1} as shown in Figure 6a. Figure 6b shows the distinctive CV curves with varying scan rates for the NiO electrode. The pseudo-rectangular CV response over the measured potential range indicates the dominant pseudocapacitive nature of the electrode in

both positive and negative potentials. It is noticeable that the CV curve remains quasi-rectangular in shape even at ultra-fast scan rate of 1000 mVs^{-1}, implying rapid charge transport in the electrode surface and more active sites were effectively involved in redox reaction. This CV result demonstrated the high rate capability of the electrode material in organic electrolyte when compared to the conventional alkaline electrolyte. Further increasing the scan rate above 500 mVs^{-1}, the CV curves show an inadequate ion intercalation on the electrode surface, which is also consistent with the earlier reports.[30,40] This result was further confirmed by the charge-discharge measurement at different current density and is presented in Figure 6c and d. Nearly linear and triangular charge-discharge curve at different current density ranging from 1 to 3.5 Ag^{-1} indicate excellent capacitive characteristic of the electrode in the organic electrolyte. The corresponding specific capacitance of the symmetric cell was calculated using the same relation described for three electrode system. The average specific capacitance of the electrode was found to vary from 34.9 to 17.7 Fg^{-1} for the corresponding current densities of 1 and 3.5 Ag^{-1} (see Fig. 6). When the current density is increased to 3.5 Ag^{-1}, nearly 50.7% of the initial capacitance has been retained, indicating a high rate and retention capability of the electrode in organic electrolyte.

The long term cyclic stability of the electrode in organic electrolyte was tested by repeated charging-discharging at 2 Ag^{-1} over 25000 cycles as shown in Figure 7a. The specific capacitance was 58% of the initial value at the end of 25000 cycles. The observed capacitance retention is quite comparable to the hybrid electrodes in organic electrolyte.[30] This may be due to good chemical compatibility of the electrode with the TEABF$_4$/PC, and good electrical conductivity between NiO and CFC. Replacement with organic electrolyte provided moderate operating potential (~ 2 V), high rate capability and good cyclic stability, however the capacitor showed low specific capacitance of < 40 Fg^{-1} compared to alkaline electrolyte. The observed low specific capacitance can be explained by the limited amount of larger size electrolyte ions accessing through active mesopores in the electrode material as also observed in Refs. 32 and 40. The high rate performance of the electrode was further confirmed by electrochemical impedance spectra and is shown in Figure 7b. Nyquist plots of the symmetric cell in TEABF$_4$/PC electrolyte consists of two parts with their respective frequency regions. From the semicircle portion, an R_{ct}

value of 5 Ω was obtained and was increased to 7.3 Ω after 25000 cycles indicating excellent electrical conductivity of the electrode.

The other important parameters of the supercapacitors are their specific energy and power density. Therefore, we have calculated the energy density, $E = CV^2/2$, and power density, $P = (E/t)$, of the supercapacitors at end of their discharge cycle. Here, E is the energy density (Whkg^{-1}), P is the power density (Wkg^{-1}), C is the specific capacitance (Fg^{-1}), V is the potential (V) and t is discharge time (s) Figure 8 presents a Ragone plot for this NiO/CFC electrode material in organic electrolyte operating in the pseudocapacitance regime. A symmetric supercapacitor fabricated using the hybrid nanostructured electrodes delivered a maximum specific energy density of 19.4 Whkg^{-1} with a 1000.6 Wkg^{-1} power density. A specific energy of 9.8 Whkg^{-1} is retained at a power density of 3504 Wkg^{-1}. It is important to point out that the energy density of our symmetric supercapacitor in organic electrolyte is comparable with metal oxide based symmetric supercapcaitors.[30,41-46] Thereby, the construction of a supercapacitor using 3D networked hybrid nanostructured electrodes and the use of organic electrolyte (TEABF$_4$/PC) could be an effective way to improve the supercapacitor performance in terms of energy and power densities. However, in order to optimize the energy and power density of the NiO nanostructure, more studies are required with different organic electrolyte system over different potential ranges.

The superior electrochemical activity with high specific energy and power density in organic electrolyte together with high rate and cycling capability demonstrates high performance characteristics of this electrode material, which may be attributed to the following structural features: first, the desired ultra-thin nanocrystals assembled nanoflakes/nanoflower hybrid morphology leads to the fast electron/ion transfer within the electrode. Secondly, the stable bonding between CFC and NiO provide good electrical conductivity and mechanical integrity for the electrode. Third, the narrow pore-size distribution with larger pore volume and high surface area of NiO hybrid nanostructure offers enough void spaces for rapid and more ion diffusion, which enhanced the core-level faradaic reactions. And finally, the flexible carbon back bone further helps in reducing the volume change within the electrode during the charge/discharge process and maintained their good electrical conductivity and bonding.

Conclusions

A hierarchical 3D NiO nanoflake/nanoflower hybrid architecture on carbon fibre cloth is demonstrated as high-performance electrode material for electrochemical energy storage devices. The unique nanoflake/ nanoflower hybrid nanostructure shows excellent electrochemical activity towards supercapacitor. In non-aqueous electrolyte, NiO/CFC electrode shows a good pseudocapacitive behaviour. As a symmetric supercapacitor electrode, it delivers a maximum specific energy density of 19.4 Whkg^{-1} at a high power density of 1000.6 Wkg^{-1} in 1 M TEABF$_4$/PC at a constant current density of 1 Ag^{-1}. Furthermore, it has shown high rate capability and good electrochemical reversibility for long term. It is concluded that the superior electrochemical performance of NiO hybrid nanostructure in organic electrolyte is mainly due to their hierarchical nanoporous microstructure, larger surface area, high electrical conductivity and well proximity with flexible CFC substrate.

References

1.   M. Winter, R.J. Brodd, Chem. Rev., 104, 4245 (2004).
2.   P. Simon, Y. Gogotsi, Nat. Mater., 7, 845 (2008).
3.   J. R. Miller, P. Simon, Science., 321, 651 (2008).
4.   M. Osiak, H. Geaney, E. Armstrong, C. O'Dwyer, J. Mater. Chem. A., 2, 9433 (2014).
5.   H.B. Li, M.H. Yu, F.X. Wang, P. Liu, Y. Liang, J. Xiao, C.X. Wang, Y.X. Tong, G. Yang, Nat. Commun., 4, 18904 (2013).
6.   T. Brezesinski, J. Wang, S.H. Tolbert, B. Dunn, Nat. Mater., 9, 146 (2010).
7.   M. Toupin, T. Brousse, D. Belanger, Chem. Mater., 16, 3184 (2004).
8.   J.W. Long, B. Dunn, D.R. Rolison, H.S. White, Chem. Rev., 104, 4463 (2004).
9.   J. Wang, J. Polleux, J. Lim, B. Dunn, J. Phys. Chem. C., 111, 14925 (2007).
10.   Y. Xiang, S. Lu, S.P. Jiang, Chem. Soc. Rev. 41, 7291 (2012).
11.   Y. Gao, Y.S. Zhou, W. Xiong, L.J. Jiang, M. Mahjouri-samani, P. Thirugnanam, X. Huang, M.M. Wang, L. Jiang, Y.F. Lu, APL Materials., 1, 012101 (2013).
12.   Y.C. Chen, Y.K. Hsub, Y.G. Lina, Y.K. Lin, Y.Y. Horng, L.C. Chen, K.H. Chen, Electrochim. Acta., 56, 7124 (2011).
13.   N. Padmanathan, S. Selladurai, RSC Adv., 4, 8341 (2014).
14.   Liangdong Feng, Yufu Zhu, Hongyan Ding, Chaoying Ni J. Power Sources., 267, 430 (2014).

15.   S. Cheng, L. Yang, Y. Liu, W. Lin, L. Huang, D. Chen, C.P. Wong, M. Liu, J. Mater. Chem. A., 1, 7709 (2013).
16.   X. Peng, L. Peng, C. Wu, Y. Xie, Chem. Soc. Rev., 43, 3303 (2014).
17.   A.E. Fischer, K.A. Pettigrew, D.R. Rolison, R.M. Stroud, J.W. Long, Nano Lett., 7 281 (2007).
18.   V. Nicolosi, M. Chhowalla, M.G. Kanatzidis, M.S. Strano, J.N. Coleman, Science., 340, 1226419 (2013).
19.   G. Zhang, X.W. Lou, Adv. Mater., 25, 976 (2013).
20.   J. Zhu, J. Jiang, J. Liu, R. Ding, H. Ding, Y. Feng, G. Wei, X. Huang, J. Solid State Chem., 184, 578 (2011).
21.   J.H. Kim, K. Zhu, Y. Yan, C.L. Perkins, A.J. Frank, Nano Lett., 10, 4099 (2010).
22.   D.T. Dam, X. Wang, J.M. Lee, Nano Energy., 2, 1303 (2013).
23.   Z. Lu, Z. Chang, J. Liu, X. Sun, Nano Res., 4(7), 658 (2011).
24.   C. Yuan, J. Li, L. Hou, X. Zhang, L. Shen, X.W. Lou, Adv. Funct. Mater., 22, 4592 (2012).
25.   V. Gupta, S. Gupta, N. Miura, J. Power Sources., 195, 3757 (2010) .
26.   H. Wang, X. Wang, ACS Appl. Mater. Interfaces., 5, 6255 (2013).
27.   J. Ji, L. L. Zhang, H. Ji, Y. Li, X. Zhao, X. Bai, X. Fan, F. Zhang, R.S. Ruoff, ACS Nano., 7, 6237 (2011).
28.   J. Zhao, J. Chen, S. Xu, M. Shao, D. Yan, M. Wei, D.G. Evans, X. Duan, J. Mater. Chem. A., 1, 8836 (2013).
29.   Y. Li, Z.Y. Fu, B.L. Su, Adv. Funct. Mater., 22, 4634 (2012).
30.   Y. Qian, R. Liu, Q. Wang, J. Xu, D. Chen, G. Shen, J. Mater. Chem. A., 2, 10917 (2014).
31.   W. Lua, L. Qu, K. Henry and L. Dai, J. Power Sources., 189, 1270 (2009).
32.   Sellam, and S. A. Hashmi, ACS Appl. Mater. Interfaces., 5, 3875 (2013).
33.   E. Coadou, L. Timperman, J. Jacquemin, H. Galiano, C. Hardacre and M. Anouti, J. Phys. Chem. C., 117, 10315 (2013).
34.   F. Luan, G. Wang, Y. Ling, X. Lu, H. Wang, Y. Tong, X.X. Liu and Y. Li, Nanoscale., 5, 7984 (2013).
35.   D. T. Dam and J.M. Lee, Electrochim. Acta., 108, 617 (2013).
36.   D. McNulty, D.N. Buckley and C. O'Dwyer, J. Electrochem. Soc., 161, A1321 (2014).
37.   C.Y. Cao, W. Guo, Z.M. Cui, W.G. Song and W. Cai, J. Mater. Chem., 21, 3204 (2011).
38.   Y.G. Wang and Y.Y. Xia, Electrochim. Acta., 51, 3223 (2006).
39.   C. M. Yang, Y. J. Kim, M. Endo, H. Kanoh, M. Yudasaka, S. Iijima and K. Kaneko, J. Am. Chem. Soc., 129, 20 (2007).
40.   L. L. Zhang, X. Zhao, M. D. Stoller, Y. Zhu, H. Ji, S. Murali, Y. Wu, S. Perales, B. Clevenger and R. S. Ruoff, Nano Lett., 12, 1806 (2012).
41.   Y. Q. Zhang, X. H. Xia, J. P. Tu, Y. J. Mai, S. J. Shi, X. L. Wang and C. D. Gu, J. Power Sources 199 (2012) 413– 417.
42.   Z. H. Gao, H. Zhang, G. P. Cao, M. F. Han and Y. S. Yang, Electrochim. Acta., 87, 375 (2013).
43.   K. Liang, X. Tang and W. Hu, J. Mater. Chem., 22, 11062 (2012).
44.   H. Pang, Y. Shi, J. Du, Y. Ma, G. Li, J. Chen, J. Zhang, H. Zheng and B. Yuan, Electrochim. Acta., 85, 256 (2012).

45. Y. Tanga, Y. Liua, S. Yua, Y. Zhaoa, S. Mub and F. Gao, Electrochim. Acta., 123, 158 (2014).
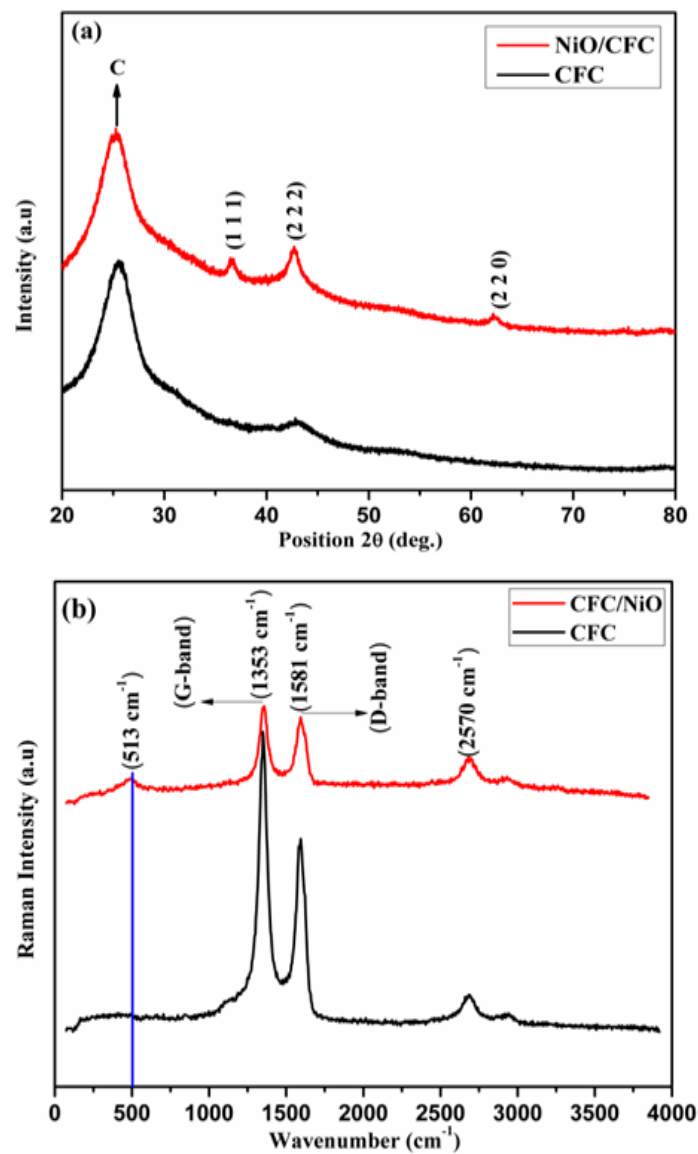46. B. K. Kim, V. Chabot and A. Yu, Electrochim. Acta., 109, 370 (2013).

Figure 1. (a) XRD pattern and (b) Raman Spectra of CFC (Black) and NiO/CFC (Red).
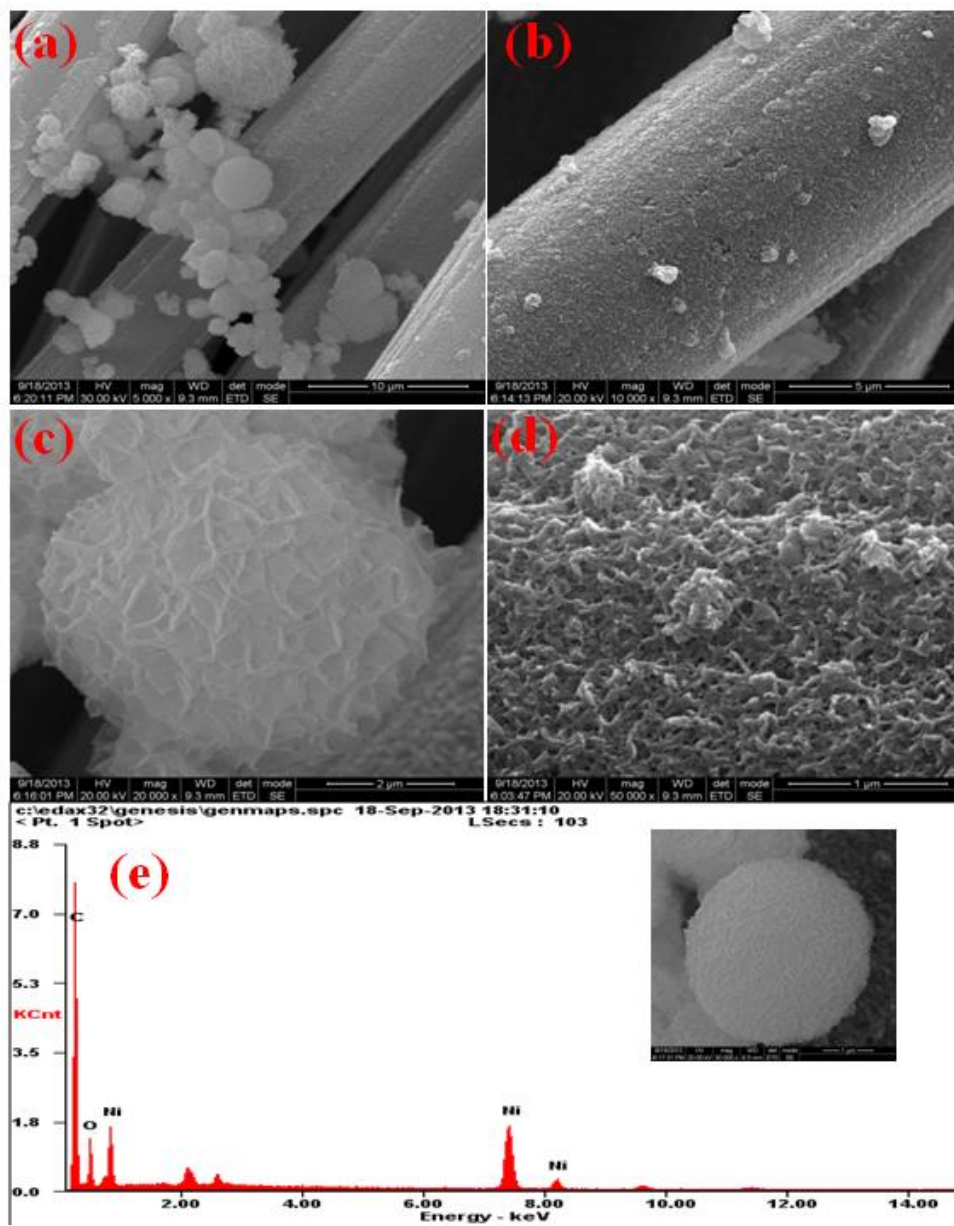
Figure 2. HRSEM (a-d) images of NiO nanoflake/nanoflower hybrid nanostructure, (e) the corresponding EDS spectrum.
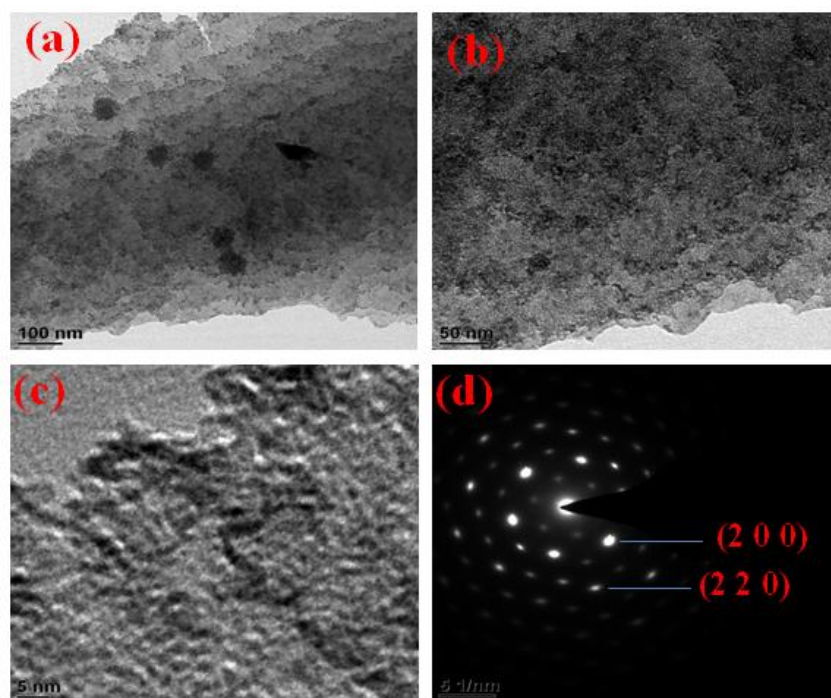
Figure 3. HRTEM (a-c) images of NiO nanoflake/nanoflower hybrid nanostructure at different magnification, (d) the corresponding SAED pattern.
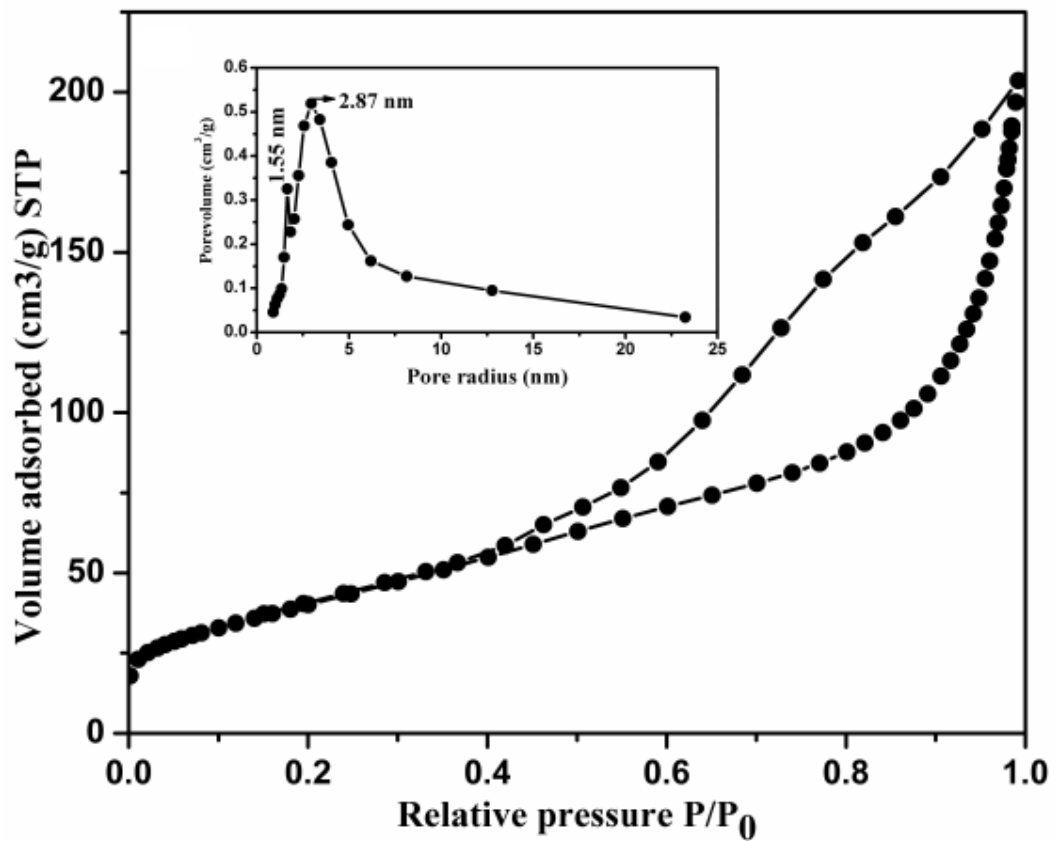
Figure 4. N_2 adsorption/desorption isotherm and inset represents the BJH pore-size distribution curve of the NiO nanostructure.
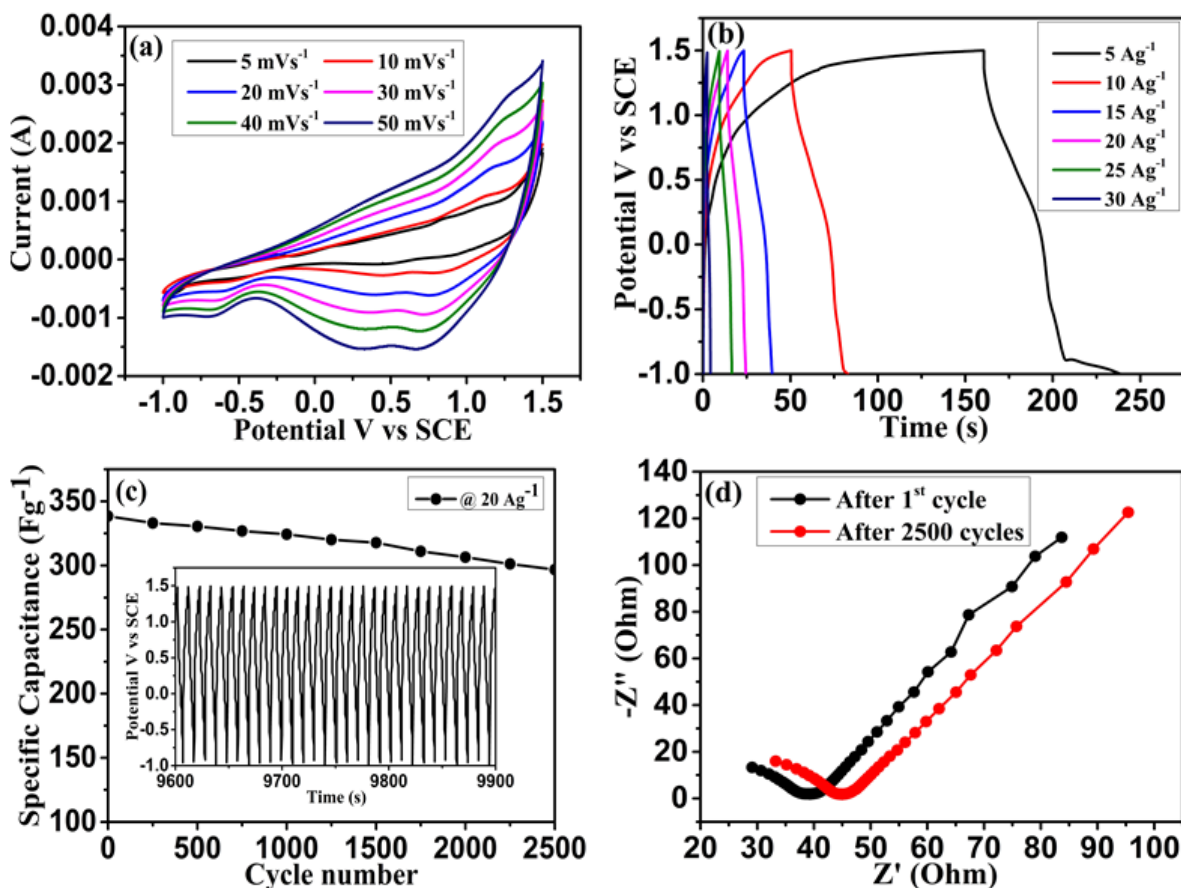
Figure 5. (a) Cyclic voltammogram of NiO/CFC hybrid nanostructure at various scan rates in organic electrolyte, (b) Charge/discharge curves of NiO/CFC electrode at various current densities, (c) Cyclic stability and continuous charge discharge at 20 Ag^{-1}(inset) (d) Nyquist plot of NiO/CFC hybrid nanostructure in 1 M TEABF$_4$/PC.
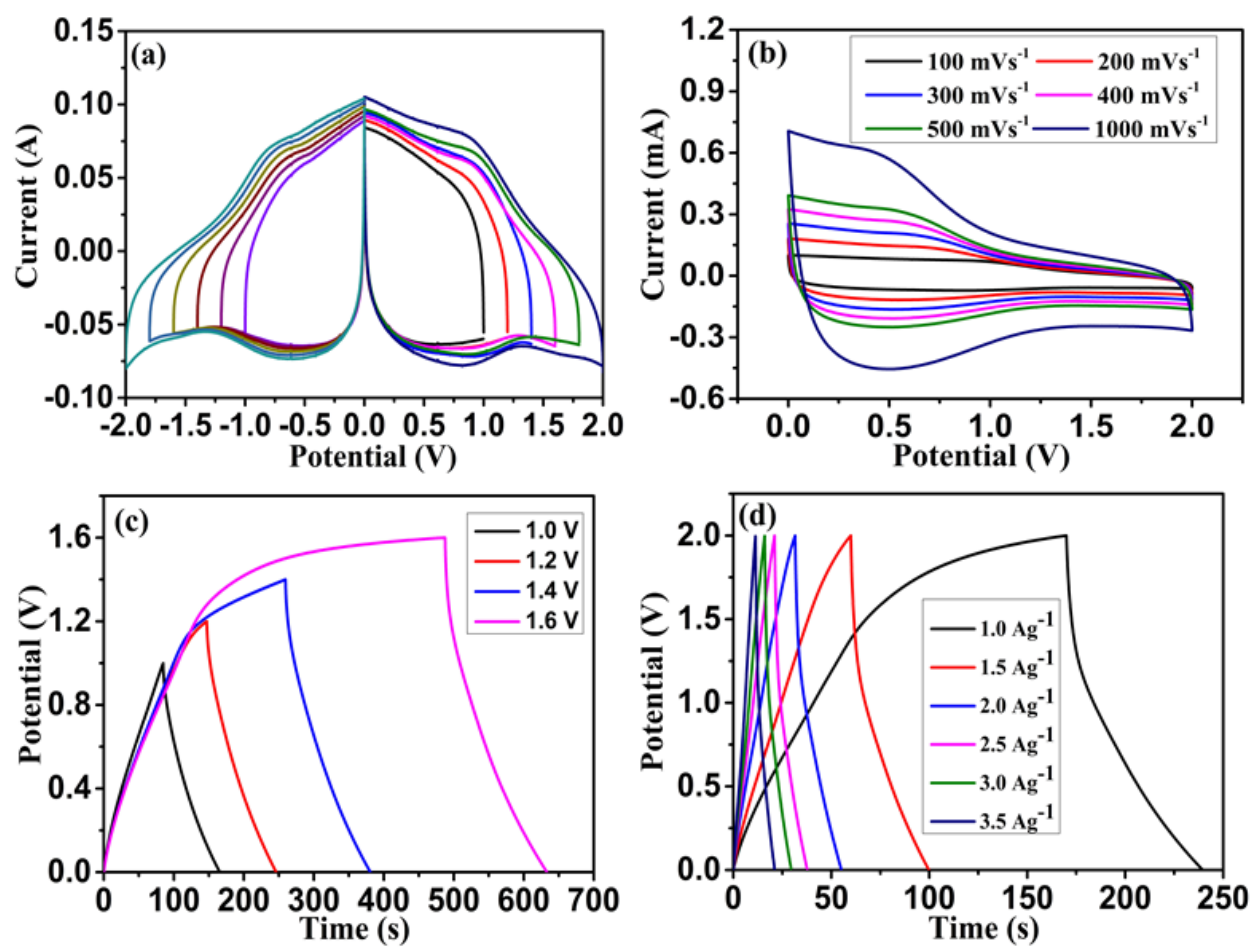
Figure 6. (a) Cyclic voltammograms of NiO/CFC symmetric supercapacitor at different potential limit in both positive and negative region in 1 M TEABF$_4$/PC, (b) CV curves at various scan rate, (c) Charge/discharge curves of the symmetric supercapacitor in different potential range at 1 Ag^{-1} current density, (d) Charge/discharge curves of the symmetric supercapacitor at various current densities in TEABF$_4$/PC.
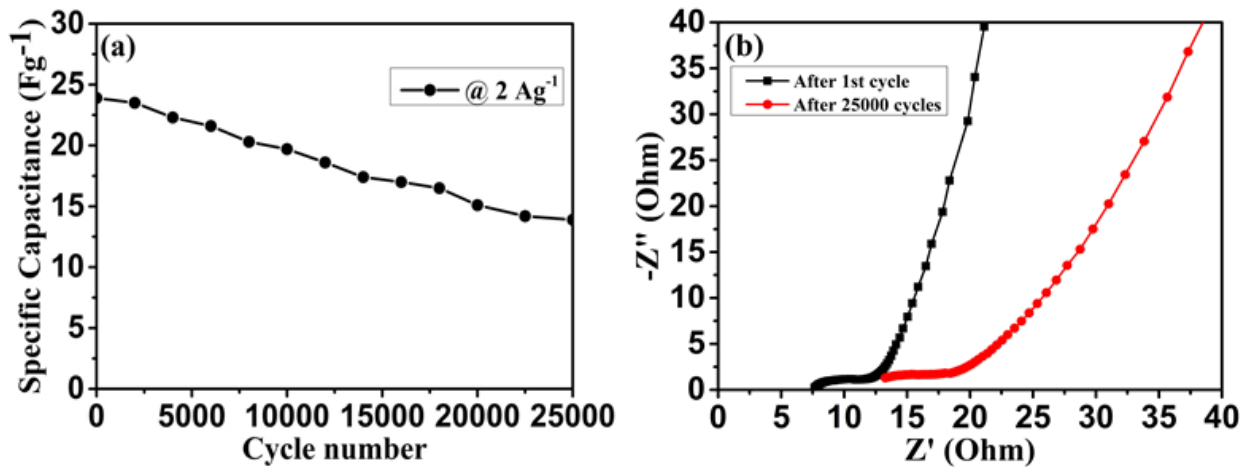
Figure 7. (a) Cyclic stability NiO/CFC based symmetric supercapacitor at 2 Ag^{-1} over 25000 cycles, (b) Nyquist plot of the symmetric supercapacitor.
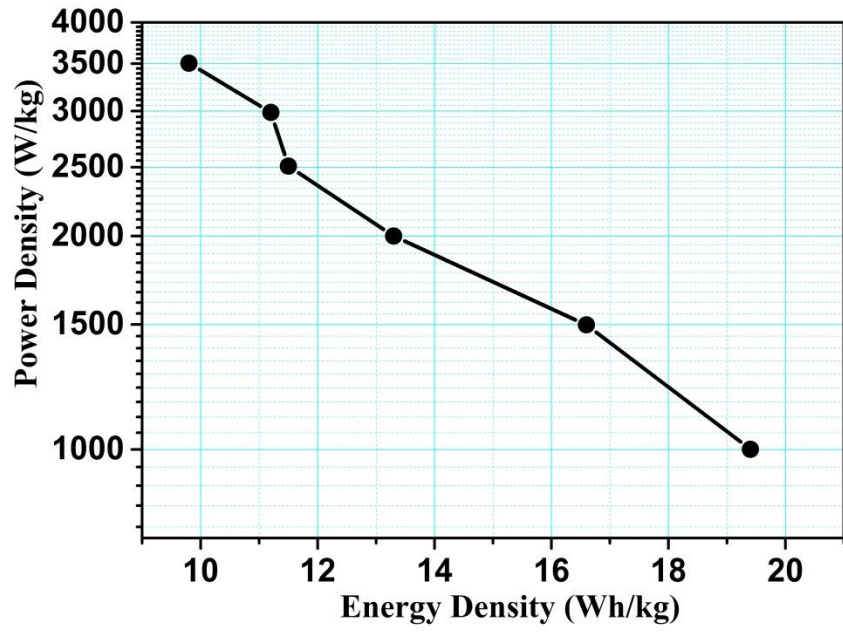
Figure 8. Ragone plot of the symmetric supercapacitor in organic electrolytes.